NANO LETTERS

LETTER

pubs.acs.org/NanoLett

Transformations of Carbon Adsorbates on Graphene Substrates under Extreme Heat

Benedikt Westenfelder,[*,†] Jannik C. Meyer,[‡,#] Johannes Biskupek,[‡] Simon Kurasch,[‡] Ferdinand Scholz,[†] Carl E. Krill, III,[§] and Ute Kaiser[‡]

[†]Institute of Optoelectronics, [‡]Central Facility of Electron Microscopy, [§]Institute of Micro and Nanomaterials, Ulm University, 89081 Ulm, Germany

Supporting Information

ABSTRACT: We describe new phenomena of structural reorganization of carbon adsorbates as revealed by in situ atomic-resolution transmission electron microscopy (TEM) performed on specimens at extreme temperatures. In our investigations, a graphene sheet serves as both a quasi-transparent substrate for TEM and as an in situ heater. The melting of gold nanoislands deposited on the substrate surface is used to evaluate the local temperature profile. At annealing temperatures around 1000 K, we observe the transformation of physisorbed hydrocarbon adsorbates into amorphous carbon monolayers and the initiation of crystallization. At temperatures exceeding 2000 K the transformation terminates in the formation of a completely polycrystalline graphene state. The resulting layers are bounded by free edges primarily in the armchair configuration.

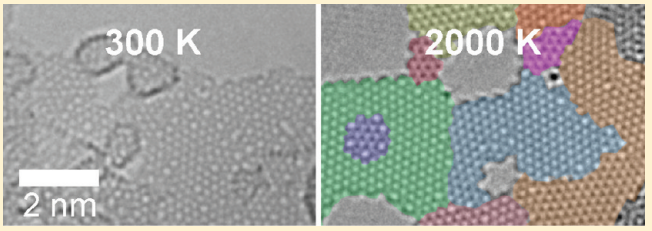

KEYWORDS: Transmission electron microscopy, in situ Joule heating, graphene, graphene edges

The recent past has witnessed tremendous gains in the capabilities of transmission electron microscopy (TEM) for exploring the atomic configuration of materials,[1] largely because of dramatic improvements in the correction of lens aberrations.[2−6] It is now possible to obtain atomic-resolution images even of light-element materials, with a reduction in radiation damage effected by the utilization of reduced acceleration voltages (see, for example, refs 7−15). Our understanding of carbon systems, such as graphene or carbon nanotubes, has significantly benefitted from these instrumental developments. When a TEM is exploited as a platform for in situ experimentation, dynamic phenomena can be studied under direct observation of the atomic structure,[16] but owing to practical limitations, such investigations have been limited so far to temperatures below about 1500 K.[17−19]

In this Letter, we report observations of heat-induced transformations of carbon adsorbates on a graphene substrate raised to temperatures in excess of 2000 K. In our experiments, a graphene sheet serves both as a quasi-transparent substrate for transmission electron microscopy[8,20−24] and as an in situ heater[25−27] that can withstand unprecedented temperatures[28] owing to its high mechanical,[29,30] thermal,[28] and chemical stability. As reference points for the local temperature, we used the melting of gold particles (diameter dependent), the transition from amorphous to crystalline silicon nitrided (1600 K), and the evaporation of SiN (2000 K).[31] The experimental concept and thermal calibration have been described in greater detail previously.[31] In brief, a graphene sheet is transferred onto a Si/SiN membrane platform prestructured with windows and gold contacts, resulting in a TEM-compatible geometry providing an electrically contacted graphene substrate with a free-standing region for transmission of the electron beam (Figure 1). The graphene layer was studied by aberration-corrected high-resolution transmission electron microscopy (AC-HRTEM) performed by a TITAN (80-300) FEI microscope equipped with a Fischione 2510 biasing TEM holder and operated at an accelerating voltage of 80 kV. Electrical current was passed through graphene specimens by applying a voltage between the gold contacts of the sample platform, achieving a typical current density on the order of 2×10^7 A/cm^2 (assuming a graphene thickness of 0.34 nm per layer) at an applied bias of 2 V. The heat-induced transformations and dynamics of gold nanoislands deposited on the graphene by thermal evaporation reveal the local temperature of the substrate and its degree of contamination. In this Letter we focus on the initial scientific results yielded by this experimental approach.

Observations made during mild heating conditions help in the estimation of the temperature distribution for our sample geometry.[31] It is well-known that the diffusion of Au adatoms on the surface of gold nanoparticles is significant even at room temperature (RT),[32,33] leading to continuous shape changes of the particles upon heating.[34] In the case of gold nanoislands deposited on graphene, we were able to correlate a decrease in the particle surface area-to-volume ratio with an increase in

Received: June 17, 2011
Revised: October 21, 2011
Published: October 24, 2011

temperature (Figure 2a). Above a certain temperature, the first particles form liquid drops and begin to evaporate (Figure 2b,c; see video M1 in the Supporting Information).[31,35] According to theoretical predictions and experimental findings, the melting temperature depends strongly on the particle size, with gold particles ranging in diameter from 3 to 20 nm expected to melt between 800 and 1300 K.[36] We performed finite-element method (FEM) simulations to estimate the entire temperature profile in the region of free-standing graphene (see Supporting Information for details). For this purpose we took both the sample carrier geometry and the influence of the graphene substrate itself into account in the calculation, obtaining the temperature profile shown in Figure 2d.

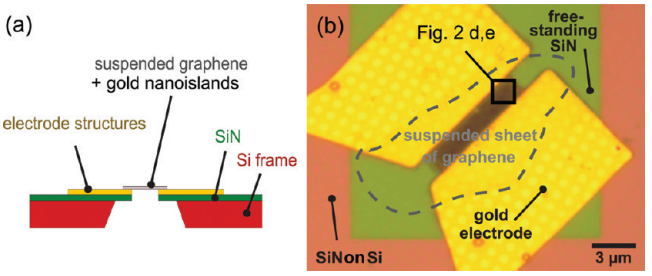

Figure 1. (a) Cross-sectional schematic illustration of the sample carrier design. (b) Optical micrograph of the electrode support structure upon which a graphene sheet is suspended. The superimposed square indicates the areas shown in panels d and e of Figure 2.

As the gold particles evaporate during TEM observation, a carbon shell with the shape of the original gold particle becomes visible. Such shells typically consist of one to three graphitic layers (Figure 2c). It appears that these layers form on the gold particles under electron irradiation and then retain their shape even after the gold particle has evaporated away. During previous in situ experiments with gold nanoparticles deposited on ultrathin amorphous carbon, it was found that intense electron-beam irradiation combined with temperatures of 425 °C and higher suffices to induce particle encapsulation with shells consisting of two−five atomic carbon layers.[34] Although the shells appear at first glance to be closed graphitic layers, our images reveal a large concentration of structural imperfections—in particular, a high degree of amorphization (Figure 2c).

The transformations in shape and phase described above were observed under continuous electron irradiation. Taking into account the fact that this irradiation is accompanied by an electron-beam-induced immobilization and enrichment of hydrocarbons,[37] we repeated the tempering procedure using the same heating current of 2×10^7 A/cm^2, but keeping large regions of graphene-supported nanoparticles unexposed to the electron beam for a duration of several minutes. Then we recorded TEM images of the previously exposed and unexposed regions. Two clear differences were observed: first, atomically clean graphene is obtained over large areas only when heat is applied prior to intense electron irradiation (Figure 2e), but not when both heat and irradiation are applied from the start simultaneously. This confirms that mobile hydrocarbon deposits are

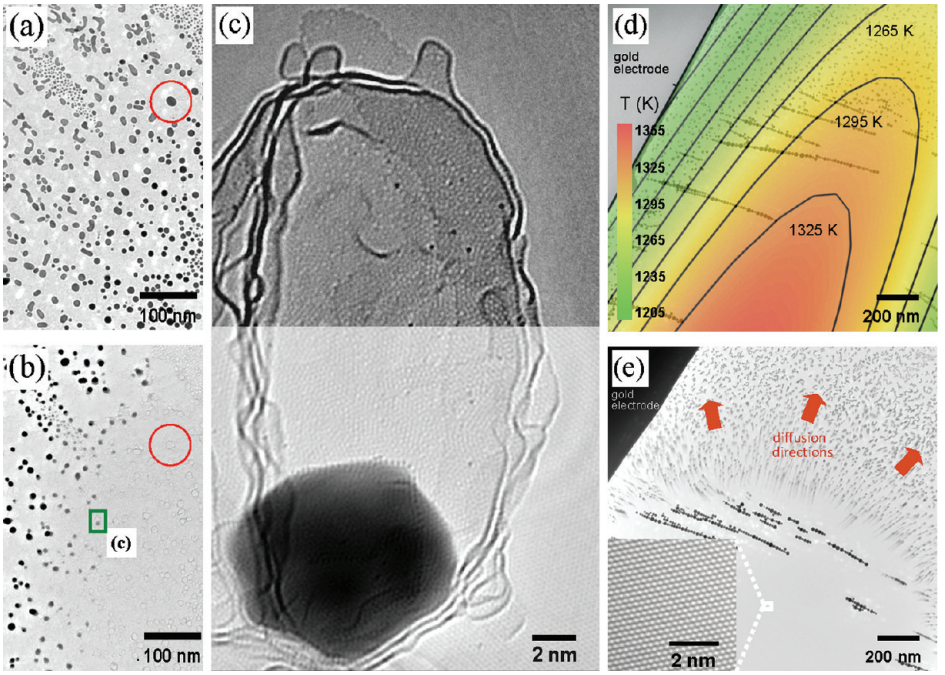

Figure 2. (a) TEM image of gold nanoislands deposited on graphene. A temperature gradient increasing from the upper left corner to the lower right is correlated with a variation in the gold particle shape. (b) The same region shown in (a) following further increase in electrical current passing through the graphene sheet. During heating, the gold particles become encapsulated in a carbon shell and finally evaporate. (c) A liquefied particle, partially evaporated inside an amorphous carbon shell (located within the green square in (b)). The contrast in the upper half of the image was increased to accentuate the atomically resolved structure of the carbon shell (after mathematical removal of the underlying graphene substrate by Fourier filtering). (d) Local temperature profile superimposed on the region shown in (e), as calculated by the finite element method (FEM). (e) Dynamically formed arrangement of gold particles on a larger region of atomically clean graphene (shown in the inset). To illustrate the migration of individual particles, we averaged the intensity of 49 images taken over a period of 100 s, resulting in the blurring of particle boundaries in the directions indicated by the red arrows.

dx.doi.org/10.1021/nl203224z |*Nano Lett.* 2011, 11, 5123–5127

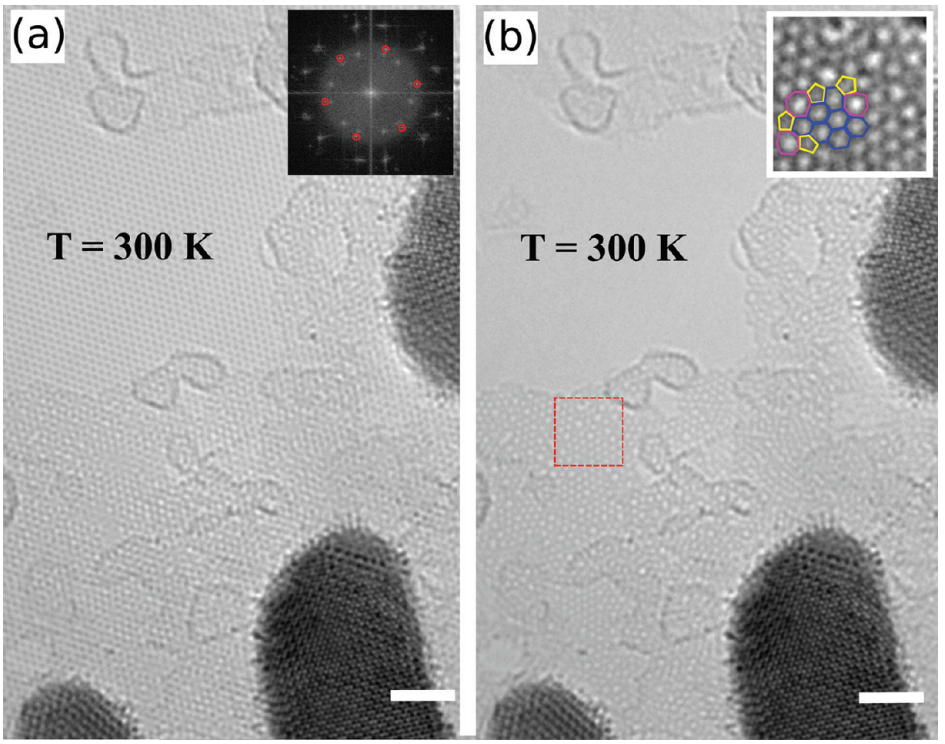

Figure 3. AC-HRTEM images of carbon and hydrocarbon adsorbates (and gold nanoparticles) on graphene (scale bars = 2 nm). (a) Unfiltered image of carbon contamination and gold particles on a bilayer graphene substrate prior to heat treatment. The inset shows an FFT of the entire image, containing diffraction peaks arising from the substrate (circled in red) and from gold. (b) Same image as in (a) after Fourier filtering of the graphene substrate. This procedure reveals the atomic structure of the amorphous carbon adsorbates, which is clearly resolved in the thinnest areas. The inset shows the region in the red box at higher magnification and contrast. The arrangement of atoms in the adsorbate can be interpreted as a random combination of carbon pentagons (indicated in yellow), hexagons (blue), and heptagons (pink). The shape of the gold nanoislands (dark contrast at lower left and right) and their absence of encapsulating carbon shells indicate that the sample had not yet seen temperatures in excess of 425 °C.

present from the start, but they can be driven off by modest heating. Evidently, upon exposure to the electron beam, the contamination is fixed in place, where it subsequently transforms under heat (as described below) without evaporating. Second, gold particles that are heated prior to electron-beam irradiation do not become encapsulated and do not leave behind a carbonaceous shell. Surprisingly, instead of melting and evaporating away, these pristine gold particles become mobile on the substrate surface, migrating as a whole at elevated temperature to form linear chainlike clusters (see video M2 in the Supporting Information). These observations will be described and discussed in detail elsewhere.

We now turn our attention to structural observations extending down to the level of individual atoms. All residual hydrocarbon deposits undergo remarkable transformations at the atomic level when exposed to high temperatures. The use of a graphene substrate allows us to observe the precise atomic configuration of the carbon adsorbates (Figures 3−5). Moreover, graphene enables locally high temperatures to be reached while simultaneously providing a stable supporting surface that does not interact strongly with the adsorbates.

A typical hydrocarbon deposit on an as-prepared graphene sample at 300 K is shown in Figure 3a. Under electron irradiation at 80 kV, mobile hydrocarbon deposits are converted to amorphous carbon, while hydrogen atoms are knocked out by electron impacts. The resulting amorphous carbon adsorbates are comparably stable under further electron-beam irradiation, and they do not easily desorb at high temperatures. In the thinnest regions,

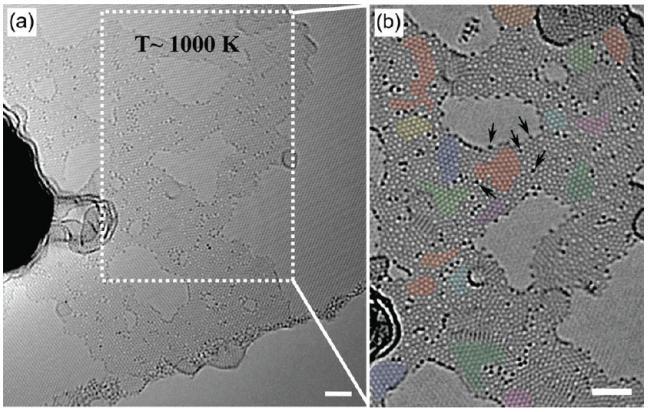

Figure 4. (a) AC-HRTEM image of single-layer carbon adsorbates on a graphene substrate at 1000 K. (b) Fourier-filtered and magnified region from (a): here, crystalline domains (shaded in color) are evident in some regions, whereas others are still amorphous. Many edge sites and vacancies are occupied by individual gold atoms (black spots, several indicated by arrows). Scale bars are 2 nm in length.

we can even resolve the atomic structure of the adsorbates (Figure 3b), which appears to be amorphous, consisting of a seemingly random arrangement of carbon pentagons, hexagons, heptagons, and other (less-frequently observed) carbon polygons.

The situation changes, however, when we apply temperatures of ∼1000 K (indicated by partial melting of the gold particles) at

dx.doi.org/10.1021/nl203224z |*Nano Lett.* 2011, 11, 5123–5127

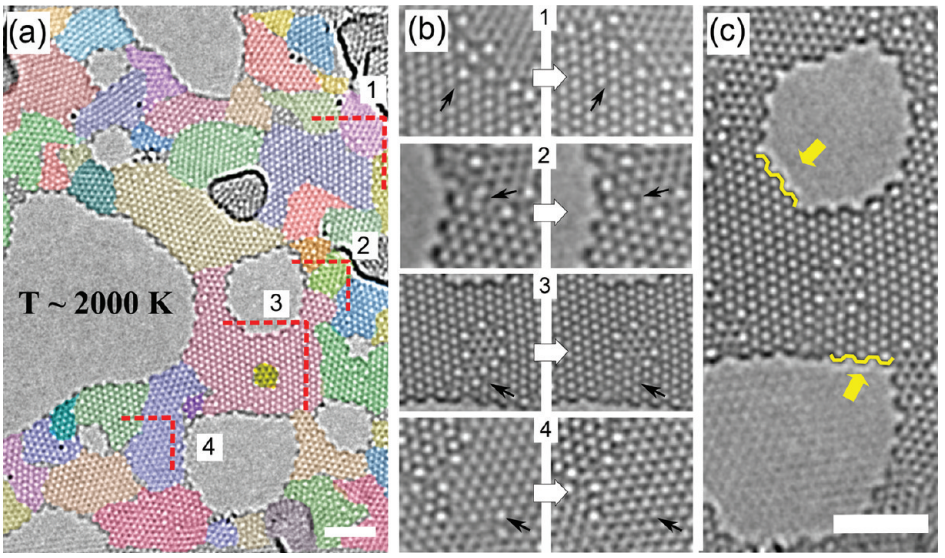

Figure 5. (a) Fourier-filtered micrograph showing fully developed grains (shaded in color) of graphene. The filtering procedure worked perfectly only in the central part of the image. This micrograph was recorded during extreme heat treatment above 2000 K, as estimated from the behavior of free-standing SiN located close to the sample (amorphous SiN is known to crystallize at 1600 K[27] and to begin decomposing around 2000 K[42]). (b) Numbered image pairs capturing dynamic rearrangements of carbon bonds during constant heating (left image = starting configuration; right image = after 100 s). (c) Markers indicate armchair-type atomic configurations at the free edges of adsorbate layers. Scale bars are 2 nm in length.

a heating current of 2×10^7 A/cm^2. First, the adsorbates reorganize into structures characterized by large areas consisting of single-layer amorphous carbon containing some crystallized domains (Figure 4). Second, gold atoms originating from the surrounding nanoislands are incorporated into the carbon matrix, as marked by the arrows in Figure 4b. Our AC-HRTEM images taken at 1000 K appear to be similar to those obtained by Turchanin et al.[38] from annealed samples characterized at RT—i.e., both crystalline and amorphous domains are observed.

However, when we raise the temperature to approximately 2000 K (the heating current is now increased by a factor of 2, and silicon nitride close to the imaged region begins to sublimate), the adsorbate transformation ends in fully crystallized graphene domains separated only by atomically sharp boundaries (Figure 5a). In other words, the amorphous carbon contamination has been transformed almost completely into a polycrystalline graphene layer situated on top of the existing graphene substrate. Image pairs 1−3 in Figure 5b illustrate various dynamic rearrangements of carbon bonds that occur at the grain boundaries, leading to greater crystallinity. The thermally induced healing of defect-like vacancies inside a crystalline grain is captured in image pair 4 of Figure 5b. We observe a polycrystalline graphene sheet having a domain size of 1−3 nm lying on top of a defect-free crystalline graphene substrate (Figure 5a). Some of the adsorbate grains are aligned with the underlying graphene lattice; however, other crystalline domains appear to be randomly oriented. Owing to the small domain size, we obtain a large number of grain boundaries within the field of view of the AC-HRTEM image. In agreement with previous studies by other authors,[39,40] we find that the grain boundaries consist of carbon pentagons and heptagons arranged in such a manner as to connect adjacent domains of differing orientation without dangling bonds.

Since the polycrystalline adsorbate layer does not completely cover the underlying substrate, we are able to observe a large number of "free edges" of individual grains. In contrast to previous room-temperature HRTEM observations of beam-induced holes in graphene,[24,42] these edges are formed and observed under high-temperature annealing. Most strikingly, most of the annealed edges exhibit an armchair-type configuration (Figure 5c). The contrast at the edges is consistent with the presence of carbon atoms: the somewhat stronger contrast of the edge atoms compared to the lattice in Figure 5 results from the contrast transfer function (CTF) of the microscope under the present conditions. In a statistical analysis of the edge configurations (see Supporting Information), 58% of all visible edges could be assigned clearly to one of the geometries calculated in ref 43. Among the classified edges, a dominant fraction—83%—exhibits the armchair conformation, 14% manifest the 5−7 reconstructed zigzag edge structure, and only 3% are found in the unreconstructed zigzag geometry.

These observations are in excellent agreement with expectations from theory (Table 1 in ref [43]): The armchair edge is the lowest energy configuration when considering the energy per atom. Furthermore, the armchair and 5−7 reconstructed zigzag are the two lowest-energy edge configurations when considering edge energy per length, with a difference of only 0.02 eV/Å. In light of these calculations, it is surprising that AC-HRTEM characterizations of free-standing graphene samples at room temperature[24,42] observed a slight preponderance of the unreconstructed zigzag configuration, especially since the energy of the latter is 0.33 eV/Å (or 1.1 eV per atom) higher than that of the armchair edge.[43] It has been speculated previously that this finding arises from the unreconstructed zigzag edges being less sensitive to radiation damage.[42] In the case of high-temperature annealing, however, the thermodynamically preferred armchair configuration appears to be most stable, as observed not only in our measurements but also in the recent investigations performed by Song et al.[44]

In summary, we have presented atomically resolved in situ TEM studies of the heat-induced evolution of hydrocarbons on graphene. Temperature profiles with maxima up to ~2000 K were obtained by passing an electrical current through a free-standing

dx.doi.org/10.1021/nl203224z |*Nano Lett.* 2011, 11, 5123–5127

graphene substrate. We found that extreme heat activates a transformation of adsorbed hydrocarbons on top of graphene into atomic monolayers of amorphous carbon, followed by crystallization. The resulting polycrystalline layers consist of free edges showing predominantly armchair configuration.

■ ASSOCIATED CONTENT

Supporting Information. Information regarding the calculation of temperature profiles, a small library of the required geometry and material parameters, as well as real-time recorded videos illustrating heat-induced nanoparticle dynamics. This material is available free of charge via the Internet at http://pubs.acs.org.

■ AUTHOR INFORMATION

Corresponding Author

*E-mail: benedikt.westenfelder@uni-ulm.de.

Present Addresses

#Department of Physics, Group Physics of Nanostructured Materials, University of Vienna, Boltzmanngasse 5, A-1090 Vienna, Austria.

■ ACKNOWLEDGMENT

This work was supported by the DFG (German Research Foundation) and the Ministry of Science, Research and the Arts (MWK) of Baden-Württemberg within the framework of the SALVE (Sub-Angstrom Low-Voltage Electron microscopy) project.

■ REFERENCES

(1) Menter, J. W. *Proc. R. Soc. London* **1956**, *236*, 119–135.
(2) Zach, J.; Haider, M. *Nucl. Instrum. Methods Phys. Res., Sect. A* **1995**, *363*, 316–325.
(3) Haider, M.; Uhlemann, S.; Schwan, E.; Rose, H.; Kabius, B.; Urban, K. *Nature* **1998**, *392*, 768–769.
(4) Krivanek, O. L.; Dellby, N.; Lupini, A. *Ultramicroscopy* **1999**, *78*, 1–11.
(5) Haider, M.; Hartel, P.; Müller, H.; Uhlemann, S.; Zach, J. *Microsc. Microanal.* **2010**, *16*, 393–408.
(6) Sawada, H.; Hosokawa, F.; Sasaki, T.; Yuasa, S.; Kawazoe, M.; Terao, M.; Kaneyama, T.; Kondo, Y.; Kimoto, K.; Suenaga, K. *Microsc. Microanal.* **2010**, *16*, 116–117.
(7) Egerton, R. F.; Li, P.; Malac, M. *Micron* **2004**, *35*, 399−409, International Wuhan Symposium on Advanced Electron Microscopy.
(8) Meyer, J. C.; Kisielowski, C.; Erni, R.; Rossel, M. D.; Crommie, M. F.; Zettl, A. *Nano Lett.* **2008**, *8*, 3582–3586.
(9) Suenaga, K.; Sato, Y.; Liu, Z.; Kataura, H.; Okazaki, T.; Kimoto, K.; Sawada, H.; Sasaki, T.; Omoto, K.; Tomita, T.; Yukihito Kondo, T. K. *Nat. Chem.* **2009**, *1*, 415–418.
(10) Suenaga, K.; Koshino, M. *Nature* **2010**, *468*, 1088–1090.
(11) Koshino, M.; Niimi, Y.; Nakamura, E.; Kataura, H.; Okazaki, T.; Suenaga, K.; Iijima, S. *Nat. Chem.* **2010**, *2*, 117–124.
(12) Krivanek, O. L.; Dellby, N.; Murfitt, M. F.; Chisholm, M. F.; Pennycook, T. J.; Suenaga, K.; Nicolosi, V. *Ultramicroscopy* **2010**, *110*, 935−945, Proceedings of the International Workshop on Enhanced Data Generated by Electrons.
(13) Kaiser, U.; Biskupek, J.; Meyer, J.; Leschner, J.; Lechner, L.; Rose, H.; Stöger-Pollach, M.; Khlobystov, A.; Hartel, P.; Müller, H.; Haider, M.; Eyhusen, S.; Benner, G. *Ultramicroscopy* **2011**, *111*, 1239–1246.
(14) Chuvilin, A.; Bichoutskaia, E.; Gimenez-Lopez, M. C.; Chamberlain, T. W.; Rance, G. A.; Kuganathan, N.; Biskupek, J.; Kaiser, U.; Khlobystov, A. N. *Nat. Mater.* **2011**, *10*, 687–692.
(15) Meyer, J. C.; Kurasch, S.; Park, H. J.; Skakalova, V.; Künzel, D.; Groß, A.; Chuvilin, A.; Algara-Siller, G.; Roth, S.; Iwasaki, T.; Starke, U.; Smet, J. H.; Kaiser, U. *Nat. Mater.* **2011**, *10*, 209–215.
(16) Ross, F. M. In *Science of Microscopy*; Hawkes, P. W., Spence, J. C. H., Eds.; Springer: New York, 2007; pp 445−534.
(17) Kamino, T.; Takahiro Sato, T. Y.; Hashimoto, T. *J. Electron Microsc.* **2005**, *54*, 505–508.
(18) Gai, P. L.; Boyes, E. D. In *EMC 2008 14th European Microscopy Congress, 5 September 2008, Aachen, Germany*; Luysberg, M., Tillmann, K., Weirich, T., Eds.; Springer: Berlin and Heidelberg, 2008; pp 481−482.
(19) Mayoral, A.; Allard, L. F.; Ferrer, D.; Esparza, R.; Jose-Yacaman, M. *J. Mater. Chem.* **2011**, *21*, 893–898.
(20) Dobelle, W. H.; Beer, M. *J. Cell Biol.* **1968**, *39*, 733–735.
(21) Meyer, J. C.; Girit, C. O.; Crommie, M. F.; Zettl, A. *Nature* **2008**, *454*, 319–322.
(22) Kaiser, U.; Chuvilin, A.; Meyer, J. C.; Biskupek, J. In *Materials Science Microscopy Conference MC2009*; Grogger, W., Hofer, F. P. P., Eds.; 2009; Vol. 3; pp 1−6.
(23) Lee, Z.; Jeon, K.-J.; Dato, A.; Erni, R.; Richardson, T. J.; Frenklach, M.; Radmilovi, V. *Nano Lett.* **2009**, *9*, 3365–3369.
(24) Chuvilin, A.; Meyer, J. C.; Algara-Siller, G.; Kaiser, U. *New J. Phys.* **2009**, *11*, 083019–1−10.
(25) Jia, X.; Hofmann, M.; Meunier, V.; Sumpter, B. G.; Campos-Delgado, J.; Romo-Herrera, J. M.; Son, H.; Hsieh, Y.-P.; Reina, A.; Kong, J.; Terrones, M.; Dresselhaus, M. S. *Science* **2009**, *323*, 1701–1705.
(26) Huang, J. Y.; Ding, F.; Yakobson, B. I.; Lu, P.; Qi, L.; Li, J. *Proc. Natl. Acad. Sci. U.S.A.* **2009**, *106*, 10103–10108.
(27) Qi, L.; Huang, J. Y.; Feng, J.; Li, J. *Carbon* **2010**, *48*, 2354–2360.
(28) Kim, K.; Regan, W.; Geng, B.; Alemán, B.; Kessler, B. M.; Wang, F.; Crommie, M. F.; Zettl, A. *Phys. Status Solidi (RRL)* **2010**, *4*, 302–304.
(29) Lee, C.; Wei, X.; Kysar, J. W.; Hone, J. *Science* **2008**, *321*, 385–388.
(30) Booth, T. J.; Blake, P.; Nair, R. R.; Jiang, D.; Hill, E. W.; Bangert, U.; Bleloch, A.; Gass, M.; Novoselov, K. S.; Katsnelson, M. I.; Geim, A. K. *Nano Lett.* **2008**, *8*, 2442–2446.
(31) Westenfelder, B.; Meyer, J. C.; Biskupek, J.; Algara-Siller, G.; Lechner, L. G.; Kusterer, J.; Kaiser, U.; Krill, C. E., III; Kohn, E.; Scholz, F. *J. Phys. D: Appl. Phys.* **2011**, *44*, 055502–1−7.
(32) Bovin, J.-O.; Wallenberg, R.; Smith, D. J. *Nature* **1985**, *17*, 47–49.
(33) Iijima, S.; Ichihashi, T. *Jpn. J. Appl. Phys.* **1985**, *24*, L125–L128.
(34) Sutter, E.; Sutter, P.; Zhu, Y. *Nano Lett.* **2005**, *5*, 2092–2096.
(35) Barnard, A. S.; Young, N. P.; Kirkland, A. I.; van Huis, M. A.; Xu, H. *ACS Nano* **2009**, *3*, 1431–1436.
(36) Buffat, P.; Borel, J.-P. *Phys. Rev. A* **2000**, *13*, 2287–2298.
(37) Rykaczewski, K.; White, W. B.; Fedorov, A. G. *J. Appl. Phys.* **2007**, *101*, 054307–1−12.
(38) Turchanin, A.; Weber, D.; Büenfeld, M.; Kisielowski, C.; Fistul, M. V.; Efetov, K. B.; Weimann, T.; Stosch, R.; Mayer, J.; Gölzhäuser, A. *ACS Nano* **2011**, *5*, 3896–3904.
(39) Huang, P. Y.; Ruiz-Vargas, C. S.; van der Zande, A. M.; Whitney, W. S.; Levendorf, M. P.; Kevek, J. W.; Garg, S.; Hustedt, J. S. A. C. J.; Zhu, Y.; Park, J.; McEuen, P. L.; Muller, D. A. *Nature* **2011**, *469*, 389–392.
(40) Yazyev, O. V.; Louie, S. G. *Nat. Mater.* **2010**, *9*, 806–809.
(41) Li, Y.; Liang, Y.; Zheng, F.; Shong, X.; Hu, Z. *J. Mater. Sci. Lett.* **1994**, *13*, 1588–1590.
(42) Giriat, C. O.; Meyer, J. C.; Erni, R.; Rossel, M. D.; Kisielowski, C.; Yang, L.; Park, C. H.; Crommie, M. F.; Cohen, M. L.; Louie, S. G.; Gettle, A. *Science* **2009**, *323*, 1705–1708.
(43) Koskinen, P.; Malola, S.; Hakkinen, H. *Phys. Sci. Lett.* **2008**, *101*, 115502.
(44) Song, B.; Scheider, G. F.; Xu, Q.; Pandraud, G.; Dekker, C.; Zandbergen, H. *Nano Lett.* **2011**, *11*, 2247–2250.